Second-harmonic generation in longitudinal epsilon-near-zero materials

M. A. Vincenti,[1,*] M. Kamandi,[2] D. de Ceglia,[3] C. Guclu,[2] M. Scalora,[4] and F. Capolino[2]
[1]*Department of Information Engineering, University of Brescia, Via Branze 38, 25123 Brescia, Italy*
[2]*Department of Electrical Engineering and Computer Science, University of California, Irvine, California 92697, USA*
[3]*AEgis Technologies Incorporated, 410 Jan Davis Drive, Huntsville, Alabama 35806, USA*
[4]*Charles M. Bowden Research Laboratory, AMRDEC, U.S. Army RDECOM, Redstone Arsenal, Alabama 35898, USA*
(Received 11 April 2017; revised manuscript received 8 June 2017; published 31 July 2017)

We investigate second-harmonic generation from anisotropic or longitudinal epsilon-near-zero materials. We find conversion efficiencies well above their isotropic counterparts owing to additional field intensity enhancement provided by the anisotropy. At the same time, anisotropic epsilon-near-zero materials are also less sensitive to the material's losses compared to the isotropic ones. In turn, these improvements become pivotal for epsilon-near-zero materials that do not possess bulk dipole-allowed quadratic nonlinearities. We predict that second-harmonic generation from a Dy:CdO/Si multilayer with longitudinal epsilon-near-zero properties can exceed the conversion efficiency of a homogeneous Dy:CdO slab of equivalent thickness by at least 20 times for almost any angle of incidence.

DOI: 10.1103/PhysRevB.96.045438

I. INTRODUCTION

Epsilon-near-zero (ENZ) materials initially gained significant attention owing to their peculiar properties, such as their ability to control antenna directivity [1,2], or to realize perfect coupling through electromagnetic tunneling in subwavelength, low-permittivity regions [3,4]. More recently, they have been also shown to be promising platforms to boost the efficiency of nonlinear optical interactions such as harmonic generation, optical bistability, and soliton excitation [5–10]. Nonlinear processes are in fact favored by the availability of high local fields, achieved when a transverse-magnetic (TM) electric field impinges obliquely on a planar ENZ film [11]. ENZ materials may be either natural or artificially engineered (metamaterials). Any natural material displays zero-crossing points for the real part of the dielectric permittivity in the vicinity of either the plasma or interband transition frequencies. For example, semiconductors such as GaAs and GaP have their zero-crossing points in the ultraviolet, metals (Au, Ag, Cu) show them in the visible, while oxides [indium tin oxide (ITO), Al-doped ZnO (AZO)] have their zero crossings in the infrared regime. Recently, ITO and AZO have been used to observe second- and third-harmonic (SH and TH) generation [12–14], as well as an enhancement of nonlinear refractive indices [15,16]. The advantage of engineering ENZ materials relies on the possibility of tuning the ENZ wavelength by properly designing the shape and dimension of the metamolecule, i.e., the unit cell of a metamaterial. The main limitation for field enhancement in both natural and artificial ENZ materials is related to absorption [17,18]. In order to overcome this issue, loss-compensation techniques have been proposed. For example, a critical reduction of the imaginary part of the dielectric permittivity in proximity of the zero-crossing region has been shown to be possible by including active materials in the lattice of plasmonic-nanoparticle arrays [19–22]. However, a practical realization of such structures is still technologically challenging. Here, we propose a different path to improve field enhancement and efficiency of nonlinear optical processes in ENZ media, without resorting to loss-compensation mechanisms. The idea is to exploit planar films of anisotropic ENZ films, namely, longitudinal ENZ or LENZ.

LENZ have been investigated for their abilities to achieve perfect light bending [23,24], angular filtering and polarization control [25], coherent perfect absorption [26], and to control leaky wave radiation [27]. Very recently, it has been theoretically demonstrated that a TM-polarized field obliquely incident on a LENZ film produces a stronger field intensity enhancement (FIE) than its isotropic ENZ (IENZ) counterpart [28], and that it might therefore lead to stronger nonlinear processes. LENZ media also present other advantages over IENZ ones, such as a weaker sensitivity of the FIE to the slab thickness, and a broader operational regime in terms of the angle of incidence [28]. These characteristics are generally desirable in practical implementations of nonlinear optical devices. Moreover, as demonstrated in Ref. [28], the presence of anisotropy circumvents damping and improves field enhancement without resorting to loss-compensation techniques.

With the intent of clarifying the differences between IENZ and LENZ for nonlinear processes, we investigate second-harmonic generation (SHG) from a homogeneous slab of LENZ and compare the radiated harmonic signal with that produced from a homogeneous IENZ film. Then, we move into a more realistic scenario, in which we discuss SHG from a structured LENZ medium obtained by alternating silicon films with dysprosium-doped cadmium oxide (Dy:CdO) films in a periodic multilayer stack. Dy:CdO is an infrared ENZ material with very low absorption losses: The imaginary part of the relative permittivity is $\sim$0.1 at the zero-crossing wavelength of the real part of the permittivity [29]. The proposed multilayer combines the advantage of an inherently low-damping ENZ material (Dy:CdO) with the additional benefits introduced by the anisotropy, i.e., a larger field enhancement, improved angular tolerance, and less sensitivity to thickness and losses. Since none of the materials in the multilayer possesses a dipole-allowed, quadratic bulk nonlinearity, we evaluate the effective second-order response that arises from symmetry

*Corresponding author: maria.vincenti@unibs.it

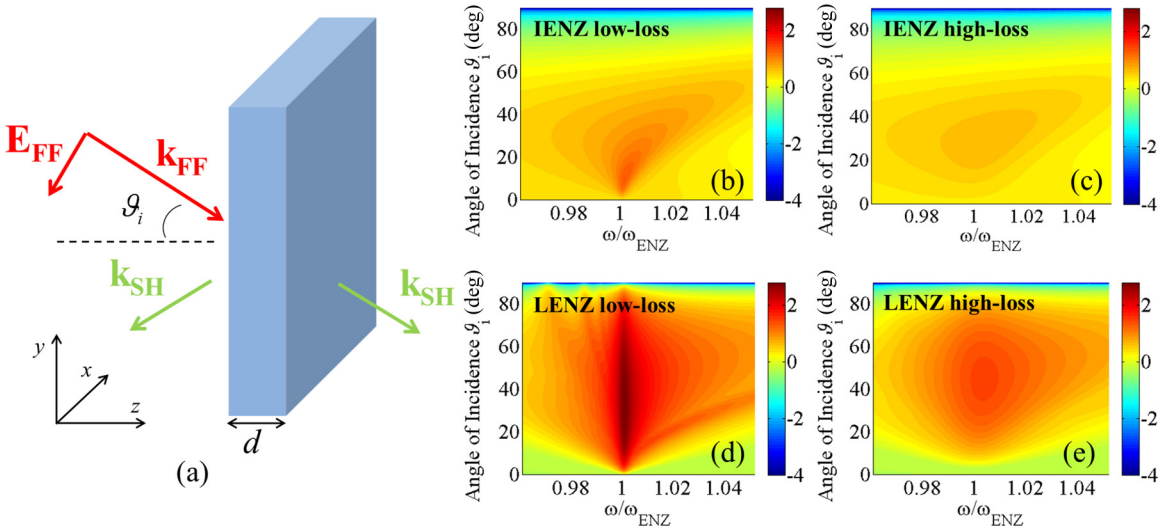

FIG. 1. (a) Sketch of the structure under investigation: A TM-polarized pump with electric field $\mathbf{E}_{\mathrm{FF}}$ and wave vector $\mathbf{k}_{\mathrm{FF}}$ impinges on a slab of thickness d with angle ϑ_i and produces forward and backward second-harmonic fields with wave vectors $\mathbf{k}_{\mathrm{SH}}$; logarithmic plot of the maximum FIE as a function of the angle of incidence and normalized frequency for a (b) IENZ slab in the low-loss scenario ($\gamma/\omega_p = 10^{-3}$) and (c) high-loss scenario ($\gamma/\omega_p = 10^{-2}$). The same calculations have been performed for a LENZ slab with (d) low loss ($\gamma/\omega_p = 10^{-3}$) and (e) high loss ($\gamma/\omega_p = 10^{-2}$).

breaking at the interfaces, modeled by means of second-harmonic (SH) current density sources that take into account volume and surface contributions from magnetic dipoles (Lorentz force) and convective nonlinear sources [30,31]. Our findings reveal that the enormous field enhancement achieved in the LENZ configuration leads to exceptional conversion efficiencies without resorting to any resonant mechanism. A comparison with the SHG radiated from a homogeneous Dy:CdO slab also suggests that a different class of nonlinear devices that does not rely on bulk nonlinearities may be envisioned. The peculiar ability of LENZ materials to provide high FIE values even in the presence of losses [28] makes them appealing for several nonlinear applications, such as second-harmonic generation, sum- and difference-frequency generation, spontaneous parametric down conversion, optical parametric amplification, bistability, and switching, in key photonic platforms based on centrosymmetric materials, such as Si and Si-on-insulator (SOI).

II. SECOND-HARMONIC GENERATION FROM IENZ AND LENZ

We start our investigation by considering a slab of material illuminated by a TM-polarized field at a variable angle ϑ_i [see Fig. 1(a)] and sweep the fundamental frequency (FF) wavelength in the vicinity of the zero-crossing point of the real part of the permittivity. The film thickness is set to $d = \lambda_0/3$, where λ_0 is the wavelength where the real part of the permittivity is equal to zero. In order to achieve an effective comparison between an IENZ and a LENZ material, we assume the low-intensity diagonal components of the permittivity tensor at the FF to be $\varepsilon_{x,\mathrm{FF}} = \varepsilon_{y,\mathrm{FF}} = \varepsilon_{z,\mathrm{FF}} = \varepsilon_\infty - \omega_p^2/(\omega_{\mathrm{FF}}^2 + i\omega_{\mathrm{FF}}\gamma)$ for the IENZ, while $\varepsilon_{x,\mathrm{FF}} = \varepsilon_{y,\mathrm{FF}} = \varepsilon_{t,\mathrm{FF}} = \varepsilon_\infty$ and $\varepsilon_{z,\mathrm{FF}} = \varepsilon_\infty - \omega_p^2/(\omega_{\mathrm{FF}}^2 + i\omega_{\mathrm{FF}}\gamma)$ for the LENZ. For both scenarios we assume the material to be isotropic at the SH frequency with $\varepsilon_{x,\mathrm{SH}} = \varepsilon_{y,\mathrm{SH}} = \varepsilon_{z,\mathrm{SH}} = \varepsilon_\infty - \omega_p^2/(\omega_{\mathrm{SH}}^2 + i\omega_{\mathrm{SH}}\gamma)$. In the Drude dispersion model we impose $\varepsilon_\infty = 5.5$ and consider the ratio $\gamma/\omega_p = 10^{-3}$ for a low-loss scenario and $\gamma/\omega_p = 10^{-2}$ for a high-loss scenario. For these materials the zero-crossing frequency occurs at $\omega_{\mathrm{ENZ}} = \omega_p/\sqrt{\varepsilon_\infty}$. The investigation of the linear properties of these two slabs reveals that the low-loss LENZ slab displays a maximum absorption peak of approximately 97%, while the IENZ slab reaches only 52%. However, since absorption is proportional to the imaginary part of the dielectric permittivity and the square of the electric field inside the slab, it is reasonable to expect that the LENZ slab produces a higher maximum FIE. We define field intensity enhancement below the top surface of the slab as

$$\mathrm{FIE} = \left|\frac{E_z}{E_0}\right|^2,$$

where E_z is the z component of the total electric field just below the top surface of the slab and E_0 is the incident electric field in the absence of the slab at the same place. Indeed, in the low-loss regime we observe a maximum FIE of ∼30 in the IENZ slab and ∼680 in the LENZ slab [Figs. 1(b) and 1(d)]. These values reduce to ∼4.5 (IENZ) and ∼20 (LENZ) in the high-loss scenario [Figs. 1(c) and 1(e)]. As detailed in Ref. [28], the superior performance of the LENZ originates from the fact that its losses may be overcome by simply enlarging the transverse (to the z-axis) permittivity ($\varepsilon_{t,\mathrm{FF}} = \varepsilon_{x,\mathrm{FF}} = \varepsilon_{y,\mathrm{FF}}$), as FIE is proportional to it, i.e.,

$$\mathrm{FIE} \propto \frac{|\varepsilon_{t,\mathrm{FF}}|}{|\varepsilon_{n,\mathrm{FF}}|}.$$

Note that the longitudinal permittivity is complex due to losses and considering its representation in terms of its real and imaginary parts, $\varepsilon_{n,\mathrm{FF}} = \varepsilon_{z,\mathrm{FF}} = \varepsilon'_{n,\mathrm{FF}} + i\varepsilon''_{n,\mathrm{FF}}$, under the LENZ condition the imaginary part does not vanish. Hence in a LENZ material the maximum field intensity enhancement

is FIE $\propto |\varepsilon_{t,\mathrm{FF}}|/|\varepsilon''_{n,\mathrm{FF}}|$. This highlights why the presence of losses may be overcome by increasing the transverse permittivity $|\varepsilon_{t,\mathrm{FF}}|$.

Another important difference between the behavior of the two slabs is the broader angular and frequency response obtained for the LENZ material. In other words, the LENZ slab shows higher FIE values for a much wider set of incidence angles and for a larger frequency range in the vicinity of the zero-crossing point. These characteristics are preserved both in the low-loss ($\gamma/\omega_p = 10^{-3}$) and high-loss ($\gamma/\omega_p = 10^{-2}$) regimes. One may thus infer that under most circumstances a LENZ slab will outperform the IENZ for nonlinear processes, even in the presence of higher damping values.

We assume that our slabs do not possess dipole-allowed, quadratic bulk nonlinearity. Therefore, to account for second-order nonlinear effects, we evaluate the effective second-order response that arises from symmetry breaking at the interface, modeled by means of second-harmonic (SH) current density sources that take into account the volume and surface contributions from magnetic dipoles (Lorentz force) and convective nonlinear sources [30,31]. The SH electromagnetic problem is then solved, by means of a commercial finite-element method, as outlined in Refs. [7,9]. In particular, SH current density sources are introduced as the superposition of two terms: a volume current $\mathbf{J}_{\mathrm{vol}}$ and a surface current $\mathbf{J}_{\mathrm{surf}}$. These currents can then be linked to the FF electric field and to the free-electron hydrodynamic parameters as follows [7,32,33],

$$\hat{\mathbf{n}} \cdot \mathbf{J}_{\mathrm{surf}} = i \frac{n_0 e^3}{2m_*^2} \frac{3 + \varepsilon_{\mathrm{FF}}}{(\omega + i\gamma)^2(2\omega + i\gamma)} E_{n,\mathrm{FF}}^2, \quad (1)$$

$$\hat{\mathbf{t}} \cdot \mathbf{J}_{\mathrm{surf}} = i \frac{2n_0 e^3}{m_*^2} \frac{1}{(\omega + i\gamma)^2(2\omega + i\gamma)} E_{n,\mathrm{FF}} E_{t,\mathrm{FF}}, \quad (2)$$

$$\mathbf{J}_{\mathrm{vol}} = \frac{n_0 e^3}{m_*^2} \frac{1}{\omega(\omega + i\gamma)(2\omega + i\gamma)} \times \left[\frac{\gamma}{\omega + i\gamma} (\mathbf{E}_{\mathrm{FF}} \cdot \nabla)\mathbf{E}_{\mathrm{FF}} - \frac{i}{2} \nabla(\mathbf{E}_{\mathrm{FF}} \cdot \mathbf{E}_{\mathrm{FF}}) \right], \quad (3)$$

where $n_0 = \varepsilon_0 m_* \omega_p^2 / e^2$ is the free-electron density, the effective electron mass is assumed to be $m_* = m_e$, and e is the elementary charge. ω_p and γ are the free-electron plasma frequency and the electron gas collision frequency, respectively. Their value has been chosen so that $\gamma/\omega_p = 10^{-3}$ for the low-loss regime and $\gamma/\omega_p = 10^{-2}$ for the high-loss regime. $\varepsilon_{\mathrm{FF}}$ is the relative permittivity at the FF, ω is the angular frequency of the FF field, $\mathbf{E}_{\mathrm{FF}}$ is the FF electric field phasor, and $\hat{\mathbf{n}}$ and $\hat{\mathbf{t}}$ are unit vectors pointing in directions outward normal and tangential to the slab surface, respectively. Moreover, $E_{n,\mathrm{FF}}$ and $E_{t,\mathrm{FF}}$ are the normal and tangential components of the FF electric field in the local boundary coordinate system defined by $\hat{\mathbf{n}}$ and $\hat{\mathbf{t}}$, respectively, and are evaluated inside the slab region. SH conversion efficiency is calculated either at the transmission or reflection side as the z component of the time-averaged Poynting vector S_z^{SH} at the SH frequency, normalized by $I_{\mathrm{FF}} \cos(\vartheta_i)$, where $I_{\mathrm{FF}} = 1\ \mathrm{GW/cm^2}$ is the input pump irradiance.

The calculations of total SHG (transmitted plus reflected) from the IENZ slab in the low- and high-loss regimes are shown in Figs. 2(a) and 2(b), respectively, while the same

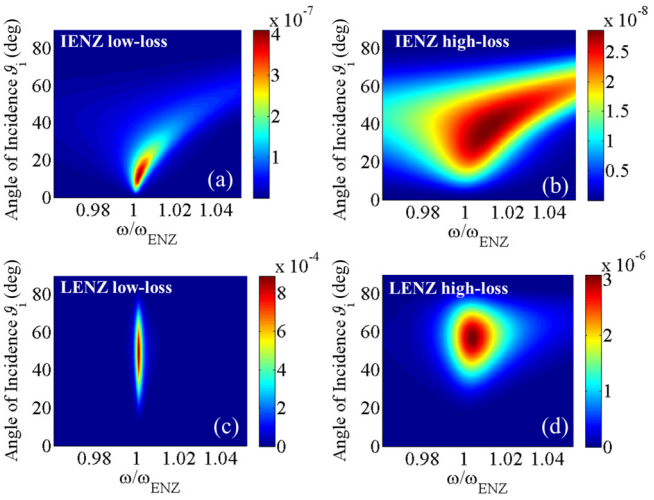

FIG. 2. SH conversion efficiency as a function of the angle of incidence and normalized fundamental frequency for an (a) IENZ slab with $\gamma/\omega_p = 10^{-3}$ (low-loss case) and (b) $\gamma/\omega_p = 10^{-2}$ (high-loss case). The same calculations have been performed for a LENZ slab with (c) $\gamma/\omega_p = 10^{-3}$ (low-loss case) and (d) $\gamma/\omega_p = 10^{-2}$ (high-loss case). Note the much higher efficiency pertaining to the LENZ cases.

calculations performed for the LENZ slab are shown in Figs. 2(c) and 2(d). The following striking differences may be found among these structures: (i) The LENZ slab produces a total SHG three orders of magnitude higher than a IENZ slab of the same thickness when operating in the low-loss regime [see the maps in Figs. 2(a) and 2(c)]; (ii) in the high-loss regime LENZ still shows a much stronger SHG than the IENZ, and the *improvement* is two orders of magnitude (instead of three as in the low-loss regime) [see the maps in Figs. 2(a) and 2(c)]; (iii) as we inferred from the linear analysis, the introduction of the anisotropy in the permittivity of the slab allows one to partially circumvent the losses of the slab, obtaining a higher SHG for the high-loss LENZ when compared to the low-loss IENZ [see the maps in Figs. 2(a) and 2(d)]; (iv) even though the maximum FIE for the LENZ slab has a broader response both in terms of angle of incidence and frequency [see Figs. 1(b)–1(e)], SHG from LENZ has a more selective profile in terms of pump frequency excitation than the IENZ material. We also note that the introduction of the anisotropy pushes the SHG peak towards greater incident angles but does not alter significantly the cone of angles that allow obtaining the best performance from all structures.

III. SECOND-HARMONIC GENERATION FROM Dy:CdO MULTILAYER STACK

We now consider a practical implementation of the concept described in the previous section. In particular, we compare the nonlinear behavior of a structured LENZ slab with a homogeneous IENZ slab. As the IENZ medium we consider a slab of Dy:CdO. This material has been investigated as a plasmonic material for the midinfrared range [29] and displays a zero-crossing point at $\lambda \sim 1867$ nm under the doping conditions described in Ref. [29]. Moreover, Dy:CdO is characterized by a smaller damping in the ENZ region than

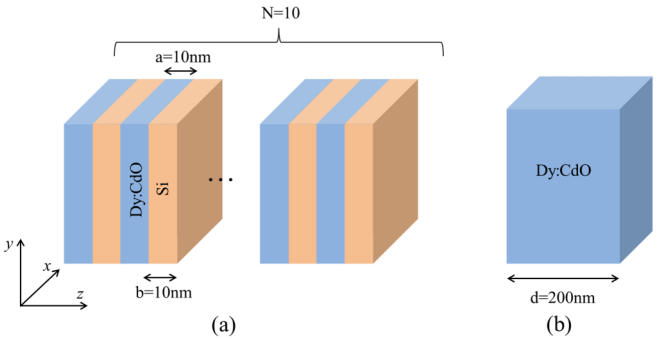

FIG. 3. (a) Sketch of the multilayer with LENZ properties: $N = 10$ periods of Dy:CdO ($a = 10$ nm) and Si ($b = 10$ nm) are alternated to obtain an anisotropic response. (b) A slab of Dy:CdO performs as an IENZ. The thickness of the slab is equal to the overall thickness of the multilayer in (a), i.e., $d = 200$ nm.

other infrared candidates, such as ITO or AZO. The LENZ metamaterial we consider, on the other hand, which is designed by alternating Dy:CdO with Si, shows a higher effective damping with respect to bulk Dy:CdO, but will provide a good example of the benefits that one may expect, in terms of nonlinear conversion efficiency, when using a LENZ material instead of a IENZ one. More specifically, we will compare the nonlinear response of ten periods of Dy:CdO/Si bilayers, with a filling ratio 50% [Fig. 3(a)], with a slab of Dy:CdO of the same total thickness of the multilayer, i.e., 200 nm [Fig. 3(b)]. The effective dielectric permittivity of the multilayer in Fig. 3(a) is calculated by adopting the Maxwell-Garnett homogenization approach and is $\varepsilon_{x,\mathrm{FF}} = \varepsilon_{y,\mathrm{FF}} = \varepsilon_{t,\mathrm{FF}} = 5.9 + i0.06$ and $\varepsilon_{z,\mathrm{FF}} = \varepsilon_{n,\mathrm{FF}} = 0.003 + i0.25$, at $\lambda_{\mathrm{FF}} = 1867$ nm. At the second-harmonic frequency ($\lambda_{\mathrm{SH}} = 933$ nm) the diagonal components of the permittivity tensor for the multilayer are $\varepsilon_{x,\mathrm{SH}} = \varepsilon_{y,\mathrm{SH}} = \varepsilon_{t,\mathrm{SH}} = 8.9 + i0.04$ and $\varepsilon_{z,\mathrm{SH}} = \varepsilon_{n,\mathrm{SH}} = 6.3 + i0.02$. These effective permittivity values have been calculated assuming Dy:CdO data from Ref. [29] and Si data taken from Ref. [34]. At the same time, the Dy:CdO slab is isotropic and characterized by the following entries for the permittivity tensor: $\varepsilon_{x,\mathrm{FF}} = \varepsilon_{y,\mathrm{FF}} = \varepsilon_{z,\mathrm{FF}} = 0.0002 + i0.13$ at $\lambda_{\mathrm{FF}} = 1867$ nm, while $\varepsilon_{x,\mathrm{SH}} = \varepsilon_{y,\mathrm{SH}} = \varepsilon_{z,\mathrm{SH}} = 4.1 + i0.02$ at $\lambda_{\mathrm{SH}} = 933$ nm [29]. We note that the Dy:CdO slab is characterized by smaller values of both the real and imaginary parts of the dielectric permittivity with respect to the multilayer effective permittivity values, at both frequencies.

The linear analysis of these two structures somehow follows what we saw for the general case described in the previous section: Even in the presence of higher damping, the maximum FIE in the artificial LENZ material, i.e., the Dy:CdO/Si multilayer stack, is higher than in the IENZ medium, i.e., 200-nm-thick Dy:CdO slab [Figs. 4(a) and 4(b)]. In particular, we find that the IENZ slab has a maximum FIE of ∼7 [Fig. 4(a)], while the LENZ multilayer shows a maximum FIE of ∼36 [Fig. 4(b)]. Under these circumstances both structures

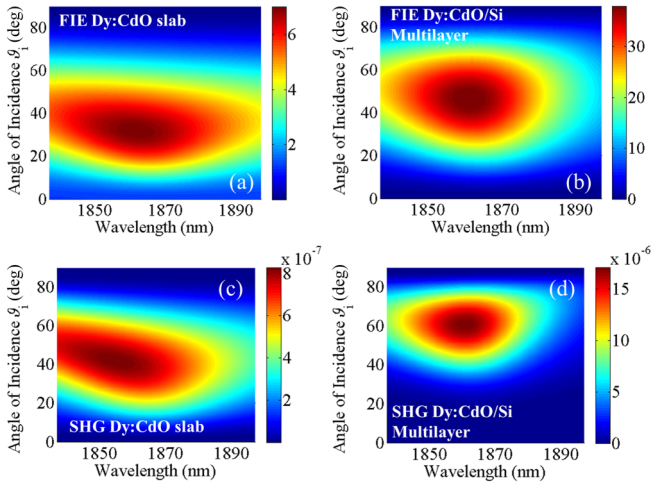

FIG. 4. (a) Plot of the maximum FIE as a function of the angle of incidence and wavelength for a 200-nm-thick Dy:CdO slab and a (b) ten-period Dy:CdO/Si multilayer; total SH conversion efficiency as a function of angle of incidence and pump wavelength from a (c) 200-nm-thick Dy:CdO slab and a (d) ten-period Dy:CdO/Si multilayer. SH conversion efficiency is 20 times higher for the multilayer case.

are more similar in terms of angular/frequency response. We ascribe this similarity to the fact that the dispersion profile of the multilayer is mostly dependent on the Dy:CdO dispersion since Si dispersion is very weak in this frequency range. On the other hand, by changing the filling ratio of the multilayer, one may alter such a response and obtain a structure with a wider (Dy:CdO filling ratio <50%) or smaller (Dy:CdO filling ratio >50%) operating bandwidth.

In order to assess the nonlinear response of the IENZ and LENZ material, we need to take a step back to understand the kinds of nonlinearities that characterize the components of these structures. CdO has a cubic crystal structure and belongs to the $Fm\bar{3}m$ crystal class [35]: It does not possess any dipolar second-order bulk nonlinearity. For simplicity, we assume that the dysprosium doping that populates the CdO lattice defects [29] neither alters its crystal structure nor does it introduce bulk nonlinear sources. Similarly, Si has a face-centered diamond-cubic crystal structure and belongs to the $Fd\bar{3}m$ crystal class [35]. Therefore, second-order dipolar nonlinearities are also absent in the bulk. In other words, the only nonlinear sources present in both systems originate from quadrupolar volume contributions and dipolar contributions due to symmetry breaking at the interfaces. In our calculations, we assume that the quadratic nonlinear response due to free electrons in Dy:CdO dominates over bound electrons of both Dy:CdO and silicon. Differently from the case illustrated in the previous section, Eqs. (1) and (2) need to be modified to take into account the presence of Si at the interface with Dy:CdO. More specifically, for the internal interfaces of the multilayer, Eqs. (1) and (2) will be modified as [33]

$$\hat{\mathbf{n}} \cdot \mathbf{J}_{\mathrm{surf}} = i \frac{n_0 e^3}{2 m_*^2 \omega_p^2 \varepsilon_B} \frac{3\varepsilon_{\mathrm{FF}}^2(\varepsilon_B - 1) + \varepsilon_B[\varepsilon_{\mathrm{FF}}(\varepsilon_B - \varepsilon_{\mathrm{FF},d}) + 3\varepsilon_B(1 - \varepsilon_{\mathrm{FF},d})]}{(\omega + i\gamma)(2\omega + i\gamma)} E_{n,\mathrm{FF}}^2, \tag{4}$$

$$\hat{\mathbf{t}} \cdot \mathbf{J}_{\mathrm{surf}} = i \frac{2 n_0 \omega e^3}{m_*^2 \varepsilon_B} \frac{\varepsilon_{\mathrm{FF}}(\varepsilon_B - 1) + \varepsilon_B\left(1 - \varepsilon_{\mathrm{FF},d}\right)}{(\omega + i\gamma)(2\omega + i\gamma)} E_{n,\mathrm{FF}} E_{t,\mathrm{FF}}. \tag{5}$$

The parameters in the equations are also modified as follows: $n_0 = \varepsilon_0 m_* \omega_p^2 / e^2$ is the free-electron density in Dy:CdO, the effective electron mass is $m_* = 0.21 m_e$ [36], and e is the elementary charge. $\omega_p = 2.4 \times 10^{15}$ rad/s and $\gamma = 2.3 \times 10^{13}\ \mathrm{s}^{-1}$ are the plasma frequency and the electron gas collision frequency in Dy:CdO, respectively [29]. $\varepsilon_{\mathrm{FF}}$ is the relative permittivity of bulk Dy:CdO at the FF, ε_B is the permittivity of the dielectric medium at the interfaces (i.e., Si at the internal interfaces and air at the first interface), and $\varepsilon_{\mathrm{FF},d}$ is the free-electron response for Dy:CdO at the FF. In the evaluation of FIE, $E_{n,\mathrm{FF}}$ and $E_{t,\mathrm{FF}}$ are assessed at the interfaces considering the values of the electric fields immediately inside the Dy:CdO regions. We stress that we did take into account only the nonlinear contributions arising from Dy:CdO free electrons and did not include the nonlinear contributions arising from Si, which are only due to bound electrons and are expected to be negligible. Such simplification allows us to compare the nonlinear behavior of a single slab of Dy:CdO with multiple layers of the same material, without introducing additional nonlinear contributions arising from other media.

We then calculate and compare the total emitted SH conversion efficiency for both structures. Figure 4(d) shows that the Dy:CdO/Si multilayer (LENZ) outperforms the CdO slab (IENZ) [Fig. 4(c)] by approximately 20 times in terms of efficiency. Moreover, owing to the peculiar field localization achieved at the surfaces of Dy:CdO in both structures (not shown), we are able to observe relatively high conversion efficiencies without resorting to any resonant mechanism nor to bulk dipolar nonlinearities. These results not only confirm the predictions of the previous section that showed how a LENZ outperforms an IENZ material even in presence of higher losses, but also prove that for the LENZ case it is not necessary to operate too close to the zero-crossing point for the real part of the effective permittivity as for the IENZ case. Indeed, the LENZ in Fig. 3(a) has an imaginary part of the dielectric permittivity twice the value for the slab of CdO. To put the SHG performance of the proposed structure in the context of conventional and emerging nonlinear materials, the pump-to-SH conversion efficiency in the 200-nm-thick Dy:CdO/Si multilayer is equivalent to that obtained in a phase-matched, 1-μm-thick slab of a nonlinear material with a bulk nonlinear coefficient equal to 30 pm/V. This means that the LENZ material has the potential to reach efficiency levels similar to those obtained in traditional nonlinear optical materials [e.g., $KTiOPO_4$ (KTP), β-BaB_2O_4 (BBO), $LiNbO_3$ [37]], in nanolaminates fabricated with atomic layer deposition [38], and in strained silicon waveguides [39]. We also note that because the second-harmonic-generated signal is extremely sensitive to the surrounding background material [33], by alternating Dy:CdO with a medium with a refractive index lower than Si, we can improve the overall conversion efficiency from the multilayer (not shown here). However, because the maximum FIE also depends on the choice of both materials, a case by case evaluation might be necessary to estimate the benefits of using a material with a smaller/higher refractive index.

A possible alternative approach to modify the linear and the nonlinear response of the multilayer is also to modify the filling ratio of Dy:CdO. As mentioned above, by either increasing or decreasing the amount of Dy:CdO, one is able to modify

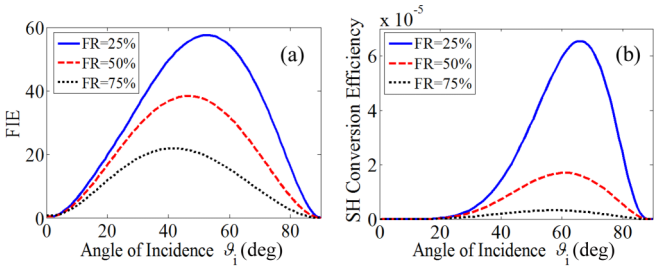

FIG. 5. (a) Plot of the maximum FIE as a function of the angle of incidence for a ten-period Dy:CdO/Si multilayer with FR = 25% (blue, solid line), 50% (red, dashed line), and 75% (black, dotted line); (b) total SH conversion efficiency as a function of angle of incidence for a ten-period Dy:CdO/Si multilayer.

the operational bandwidth of the device. As an example we compare three multilayers composed of ten periods of Dy:CdO and Si with filling ratios FR = 25%, 50%, and 75%, where the filling ratio is defined as FR $= a/(a+b)$ [see Fig. 3(a)]. The plots of maximum FIE and SHG are shown in Figs. 5(a) and 5(b), respectively. These plots assume an incident pump wavelength tuned at $\lambda_{\mathrm{FF}} = 1861$ nm and $I_{\mathrm{FF}} = 1\ \mathrm{GW/cm^2}$.

By changing the fraction of Dy:CdO present in the multilayer we are altering the effective permittivity of the material in the longitudinal ($\varepsilon_n = \varepsilon_z$) and transverse ($\varepsilon_t = \varepsilon_x = \varepsilon_y$) directions, therefore modifying both linear and nonlinear responses. For these three particular cases we move from $\varepsilon_x = \varepsilon_y = \varepsilon_t = 8.9 + i0.03$, $\varepsilon_z = \varepsilon_n = 0.02 + i0.5$ (FR = 25%) to $\varepsilon_x = \varepsilon_y = \varepsilon_t = 5.9 + i0.06$, $\varepsilon_z = \varepsilon_n = 0.003 + i0.25$(FR = 50%), and $\varepsilon_x = \varepsilon_y = \varepsilon_t = 2.9 + i0.09$, $\varepsilon_z = 0.0009 + i0.16$ (FR = 75%). We see from these values how increasing the amount of Dy:CdO in the multilayer lowers the degree of anisotropy in the system, i.e., the transverse component ε_t of the effective permittivity gets smaller. At the same time the real part of the longitudinal component of the dielectric permittivity ε_n decreases as well. As a result, the maximum FIE follows the same trend [see Fig. 5(a)], as shown also in Ref. [28]. Because SH generation in the multilayers happens mostly at the surface, an increase in the maximum FIE corresponds to an analogous behavior for the nonlinear process. Figure 5(b) shows how we can boost or lower the total radiated SH by simply changing the FR of the structure, proving the extreme flexibility of these kinds of structures and their effectiveness to overcome the limitation of IENZ materials.

We stress also that the level of doping of the Dy:CdO [29] layers provides a way to tune the epsilon-near-zero frequency and the level of damping in the Dy:CdO layers and, therefore, in the stack. For example, by simply increasing the Dy doping in the CdO from 9.94×10^{19} to $3.7 \times 10^{20}\ \mathrm{cm^{-3}}$, one can move the zero-crossing wavelength for the real part of the dielecric permittivity of Dy:CdO from 3.6 to 1.86 μm and lower the imaginary part of the dielectric permittivity at the same wavelength from 0.19 to 0.13. These parameter changes in the Dy:CdO layers in turn change the entries of the effective permittivity tensor, a Si/Dy:CdO stack with 50% FR from $\varepsilon_x = \varepsilon_y = \varepsilon_t = 5.9 + i0.09$, $\varepsilon_z = \varepsilon_n = 0.006 + i0.38$ (for doping $9.94 \times 10^{19}\ \mathrm{cm^{-3}}$) to $\varepsilon_x = \varepsilon_y = \varepsilon_t = 5.9 + i0.06$, $\varepsilon_z = \varepsilon_n = 0.003 + i0.26$ (for doping $3.7 \times 10^{20}\ \mathrm{cm^{-3}}$). Finally, we note that while small variations in the thicknesses due to fabrication

processes are not expected to alter significantly both the linear and nonlinear responses of the stack, roughness effects may impact the nonlinear response of the stack since the effective mass, damping, and scattering rate can locally change at the surfaces.

IV. CONCLUSIONS

We showed that the SH signal radiated from a LENZ material is higher than the signal radiated from a IENZ material, even in the presence of higher damping. An analysis of a system with realistic material parameters not only confirmed these findings but also suggested that the proximity of the real part of the dielectric permittivity to the zero-crossing point is not a critical condition to achieve efficient nonlinear processes, provided that anisotropy is present. We found that a ten-period Dy:CdO/Si multilayer, performing as a LENZ medium, produces a SH radiated signal approximately 20 times higher than a 200-nm-thick slab of Dy:CdO (IENZ medium). Our results suggest that the higher maximum FIE values achievable in the LENZ configuration render resonant mechanisms and bulk nonlinearities unnecessary: A 200-nm-thick LENZ multilayer produces an overall SHG efficiency of $\sim 10^{-5}$ with a pump irradiance of $1\,\mathrm{GW/cm^2}$, in line with conventional and emerging quadratic-nonlinear materials. The comparison of the nonlinear behavior of the Dy:CdO/Si multilayer with the Dy:CdO slab therefore suggests that LENZ materials may be able to overcome the limitations imposed by the damping of natural IENZ materials, therefore informing further work toward the eventual realization of a different class of nonlinear devices currently unavailable.

ACKNOWLEDGMENT

M.K., C.G., and F.C. acknowledge partial support from the National Science Foundation, Award No. NSF-SNM-1449397.

[1] S. Enoch, G. Tayeb, P. Sabouroux, N. Guérin, and P. Vincent, Phys. Rev. Lett. **89**, 213902 (2002).
[2] G. Lovat, P. Burghignoli, F. Capolino, D. R. Jackson, and D. R. Wilton, IEEE Trans. Antennas Propag. **54**, 1017 (2006).
[3] A. Alù, M. G. Silveirinha, A. Salandrino, and N. Engheta, Phys. Rev. B **75**, 155410 (2007).
[4] M. Silveirinha and N. Engheta, Phys. Rev. Lett. **97**, 157403 (2006).
[5] M. A. Vincenti, D. de Ceglia, A. Ciattoni, and M. Scalora, Phys. Rev. A **84**, 063826 (2011).
[6] A. Ciattoni and E. Spinozzi, Phys. Rev. A **85**, 043806 (2012).
[7] M. A. Vincenti, S. Campione, D. de Ceglia, F. Capolino, and M. Scalora, New J. Phys. **14**, 103016 (2012).
[8] A. Ciattoni, C. Rizza, and E. Palange, Phys. Rev. A **81**, 043839 (2010).
[9] D. de Ceglia, S. Campione, M. A. Vincenti, F. Capolino, and M. Scalora, Phys. Rev. B **87**, 155140 (2013).
[10] C. Rizza, A. Ciattoni, and E. Palange, Phys. Rev. A **83**, 053805 (2011).
[11] S. Campione, D. de Ceglia, M. A. Vincenti, M. Scalora, and F. Capolino, Phys. Rev. B **87**, 035120 (2013).
[12] D. S. Chemla and J. Zyss, *Nonlinear Optical Properties of Organic Molecules and Crystals* (Academic, New York, 1987).
[13] M. M. Fejer, G. A. Magel, D. H. Jundt, and R. L. Byer, IEEE J. Quantum Electron. **28**, 2631 (1992).
[14] J. Zyss, *Molecular Nonlinear Optics: Materials, Physics, and Devices* (Academic, New York, 1994).
[15] M. Z. Alam, I. De Leon, and R. W. Boyd, Science **352**, 795 (2016).
[16] L. Caspani, R. P. M. Kaipurath, M. Clerici, M. Ferrera, T. Roger, J. Kim, N. Kinsey, M. Pietrzyk, A. Di Falco, V. M. Shalaev, A. Boltasseva, and D. Faccio, Phys. Rev. Lett. **116**, 233901 (2016).
[17] M. A. Vincenti, D. de Ceglia, and M. Scalora, Opt. Express **21**, 29949 (2013).
[18] M. Vincenti, D. de Ceglia, V. Roppo, and M. Scalora, in *Nonlinear, Tunable and Active Metamaterials*, edited by I. V. Shadrivov, M. Lapine, and Y. S. Kivshar (Springer, Berlin, 2015), Vol. 200, p. 117.
[19] S. Campione, M. Albani, and F. Capolino, Opt. Mater. Express **1**, 1077 (2011).
[20] S. Campione and F. Capolino, Nanotechnology **23**, 235703 (2012).
[21] A. Ciattoni, R. Marinelli, C. Rizza, and E. Palange, Appl. Phys. B **110**, 23 (2013).
[22] S. Xiao, V. P. Drachev, A. V. Kildishev, X. Ni, U. K. Chettiar, H.-K. Yuan, and V. M. Shalaev, Nature (London) **466**, 735 (2010).
[23] J. Luo, P. Xu, H. Chen, B. Hou, L. Gao, and Y. Lai, Appl. Phys. Lett. **100**, 221903 (2012).
[24] B. Edwards, A. Alù, M. G. Silveirinha, and N. Engheta, J. Appl. Phys. **105**, 044905 (2009).
[25] L. V. Alekseyev, E. E. Narimanov, T. Tumkur, H. Li, Y. A. Barnakov, and M. A. Noginov, Appl. Phys. Lett. **97**, 131107 (2010).
[26] S. Feng and K. Halterman, Phys. Rev. B **86**, 165103 (2012).
[27] K. Halterman, S. Feng, and V. C. Nguyen, Phys. Rev. B **84**, 075162 (2011).
[28] M. Kamandi, C. Guclu, T. S. Luk, G. T. Wang, and F. Capolino, Phys. Rev. B **95**, 161105 (2017).
[29] E. Sachet *et al.*, Nat. Mater. **14**, 414 (2015).
[30] M. Scalora, M. A. Vincenti, D. de Ceglia, V. Roppo, M. Centini, N. Akozbek, and M. J. Bloemer, Phys. Rev. A **82**, 043828 (2010).
[31] J. E. Sipe, V. C. Y. So, M. Fukui, and G. I. Stegeman, Phys. Rev. B **21**, 4389 (1980).
[32] D. Maystre, M. Neviere, and R. Reinisch, Appl. Phys. A **39**, 115 (1986).
[33] A. Benedetti, M. Centini, C. Sibilia, and M. Bertolotti, J. Opt. Soc. Am. B **27**, 408 (2010).
[34] C. D. Salzberg and J. J. Villa, J. Opt. Soc. Am. **47**, 244 (1957).
[35] P. Patnaik, *Handbook of Inorganic Chemicals* (McGraw-Hill, New York, 2003).
[36] P. H. Jefferson, S. A. Hatfield, T. D. Veal, P. D. C. King, C. F. McConville, J. Zúñiga-Pérez, and V. Muñoz-Sanjosé, Appl. Phys. Lett. **92**, 022101 (2008).
[37] R. W. Boyd, *Nonlinear Optics* (Academic, New York, 2003).
[38] L. Alloatti *et al.*, Appl. Phys. Lett. **107**, 121903 (2015).
[39] M. Cazzanelli *et al.*, Nat. Mater. **11**, 148 (2012).